ACS Catalysis

Research Article

pubs.acs.org/acscatalysis

Impact of Nonadiabatic Charge Transfer on the Rate of Redox Chemistry of Carbon Oxides on Rutile TiO_2(110) Surface

Yeohoon Yoon, Yang-Gang Wang, Roger Rousseau, and Vassiliki-Alexandra Glezakou*

Fundamental and Computational Sciences Directorate, Pacific Northwest National Laboratory, PO Box 999, K1-83, Richland, Washington 99352, United States

Supporting Information

ABSTRACT: We present the results of a density functional theory (DFT) within the LDA+U approximation on large models of the partially reduced TiO_2(110) rutile surface to investigate the nature of charge transfer and the role of nonadiabatic effects on three prototypical redox reactions: (i) O_2 adsorption, (ii) CO oxidation, and (iii) CO_2 reduction. Charge-constrained DFT (cDFT) is used to estimate kinetic parameters for a Marcus theory rate law that accounts for adiabatic coupling effects on reaction rates. We find that for O_2 adsorption, the coupling between adiabatic states is strong, leading to fast charge transfer rates. The lowest energy structures at high coverage consist of two chemisorbed O_2^-, one adsorbed at a V_O site and the other adsorbed at an adjacent Ti_{5C} site. For CO oxidation, however, all reactions are kinetically hindered on the ground state because of the weak adiabatic coupling at the state crossing, such that one has to overcome two kinetically unfavorable charge transfer events to drive the process (nonadiabatically) on the thermal ground state. The process can be driven by photochemical means but would result in an adsorbed radical [$OCOO^-$] intermediate species. Similarly, CO_2 reduction also proceeds via a nonadiabatic charge transfer to form an adsorbed CO_2^- species, followed by a second nonadiabatic charge transfer to produce CO. Our analysis provides important computational guidelines for modeling these types of processes.

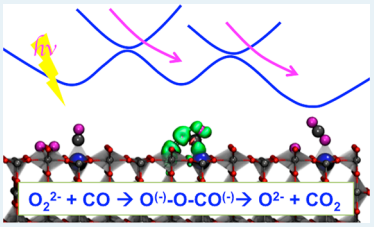

KEYWORDS: *charge transfer, carbon oxides, redox chemistry, nonadiabatic effects, rutile TiO_2, Marcus theory*

INTRODUCTION

Titanium dioxide is considered one of the technologically most promising oxides with a broad range of catalytic and photocatalytic applications.[1,2] Its ability to oxidize organic contaminants and eliminate pathogens has resulted in the emergence of numerous applications in the areas of air purification,[3,4] wastewater treatment,[5] self-cleaning glass,[6] medical implants,[7] and gas sensing,[8] and it is ubiquitously encountered in catalysis as both a support material and a catalyst. As such, there has been extensive effort devoted to the understanding of elemental processes that take place during catalytic and photocatalytic reactions on TiO_2.[9−13] The fundamental studies of the reactions on the thermodynamically stable TiO_2(110) surface of the rutile phase, in particular, have provided an unprecedented level of insight into the mechanisms of adsorption, dissociation, diffusion, and product formation.[14] In the past few years, we have been interested in the detailed modeling of reducible support materials for catalysis for which TiO_2 is a prototypical example. Our research has been aimed at using large scale electronic structure calculations to understand, at the atomic level, fundamental issues such as how charge transfer occurs at this surface and how the oxide and the supported metal particles interact to perform a given catalytic chemistry.[15] In this particular study, we will examine in detail the redox chemistry of rutile TiO_2(110) for a few well documented surface redox processes with the goal of providing general insights on which types of redox reactions can occur on this oxide, how electron transfer rate influences this chemistry, and how one properly models these processes.

Much of the thermal redox chemistry associated with this surface is governed by the presence of defects such as oxygen vacancies (V_O) or interstitial Ti atoms (Ti_{int}) residing beneath the surface or surface-bound hydroxyls (OH). See Figure 1 for a pictorial representation of the surface and nomenclature of the relevant sites. These species donate excess electrons to the TiO_2 lattice, which exist as polaronic states residing on Ti^{3+} sites. They are generally mobile through the TiO_2 lattice and are able to provide a source of charge for adsorbents, such as

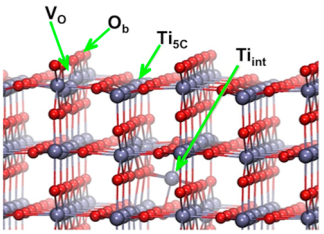

Figure 1. Illustration of TiO_2(110) surface with nomenclature of defect and reaction sites; see text for discussion.

Received: November 25, 2014
Revised: January 26, 2015
Published: January 28, 2015

DOI: 10.1021/cs501873m
ACS Catal. 2015, 5, 1764−1771

O_2, for surface reduction of species.[16−18] Although much attention has been paid to the structure and energetics of charge transfer reactions on this surface,[19−21] appreciably less attention has been paid to the kinetics of such processes[22,23] to determine which are adiabatic in nature and, thus, thermally facile or nonadiabatic and, hence, kinetically hindered and requiring either electrochemical or photoinduced charge transfer. The goal of this study is to examine and discuss these issues by means of simulation in the context of three distinct prototypical reactions: O_2 adsorption, CO oxidation, and CO_2 reduction.

The O_2 adsorption reaction has been extensively studied.[2,24−29] Our current understanding is that O_2 preferentially adsorbs at V_O sites on the TiO_2(110) surface at low coverage.[2,14,24−29] Up to two O_2 molecules are known to chemisorb per V_O site, although their charge state, the number of excess electrons involved, and their structure are still under debate. This is in part due to the inherent inability of our theoretical models to deal with charge transfer at oxide surfaces and account for the number of excess electrons that are available for surface chemistry.[30] In general, the amount of charge available at the surface determines how much of that can be transferred to the adsorbate, but long-range electrostatic interactions and band bending are not readily accounted for in electronic structure models based on finite-sized surface slabs. Recently, we addressed this issue in the context of O_2 adsorption at Ti_{5C} surface sites and concluded that thermal charge transfer is obtainable only from excess charges resulting from defects in the near-surface layers, that is, around 1 nm, corresponding to ∼2−3 TiO_2 trilayers.[30] This essentially implies that only the two excess electrons associated with an oxygen vacancy are available for O_2 adsorption. Similar conclusions were drawn by temperature-programmed and electron-stimulated desorption (TPD and ESD) studies;[26] however, it is not clear what is the chemical nature of these adsorbed species. An additional complexity arises when one compares the identical reaction on the anatase phase of TiO_2, where it has recently been shown that the analogous O_2 adsorption reaction can be hindered by a nonadiabatic charge transfer process.[31,22] Given the nature of the charge rearrangements, we ask whether nonadiabatic charge transfer effects are in play for this reaction and what impact this has on the resulting structures of the adsorbed O_2 species.

CO oxidation on rutile TiO_2 by chemisorbed O_2 at a V_O site is believed to proceed photochemically, not thermally, despite theoretical reports that show low reaction barriers and a strong thermodynamic driving force.[12,28,32−34] The reaction is thought to proceed via a hole migrating onto the adsorbed O_2^{2-}, creating an adsorbed O_2^- at the V_O site.[35] It can then combine with an adsorbed CO molecule and readily produce CO_2, which easily desorbs. The remaining O^- accepts an electron back from the surface effectively becoming an O^{2-}, and heals the V_O defect. Recently, however, it was shown by photostimulated desorption studies that there exists an unknown transient intermediate species that has a long lifetime and requires a second photon before CO_2 can be ejected.[34] Here, we ask (i) Why this process does not proceed thermally, despite the favorable thermodynamics and reported low activation barriers? (ii) What is the nature of the proposed intermediate, and what types of charge transfer (electrons or holes) are necessary to stabilize them?

Finally, we will consider CO_2 adsorption and dissociation at a V_O site, leading to healing of the vacancy and CO desorption. Thermally, CO_2 is known to desorb intact from a V_O site; however, like CO oxidation, this reaction is known to be thermodynamically stable. Nonetheless, it can be induced only by the injection of electrons (with ∼1 V external bias).[36−38] Given the fact that there are two electrons available in the vicinity of the V_O site, it is reasonable to ask why this process does not proceed thermally. We will show that the root of this phenomenon lies in the nonadiabatic charge transfer between adsorbates and surface.

In this paper, we employ density functional theory (DFT) within LDA+U approximation on large surface slab models of the rutile TiO_2(110) surface to investigate the nature of the chemical reactivity of three prototypical reactions. Charge-constrained DFT is used to estimate kinetic parameters for charge transfer as required for a Marcus theory rate law in a similar fashion, as was previously applied to the study of the reaction of diols on the same surface.[39] We will show that for O_2 adsorption, charge transfer is fast and the lowest energy structures at high coverage consist of two chemisorbed O_2^-: one adsorbed at a V_O site and the other adsorbed at an adjacent Ti5C site. For CO oxidation, however, all reactions are kinetically hindered on the ground state because of a weak nonadiabatic coupling at the transition state, such that one has to overcome two kinetically unfavorable charge transfer events to drive the process on the thermal ground state via an adsorbed radical [$OCOO^-$] species. Likewise, CO_2 reduction requires two slow charge-transfer steps to form an adsorbed CO_2^- species, followed by a second nonadiabatic electron transfer to produce CO. We will conclude this study with general observations about the nature of the charge transfer steps and implications for computational studies of catalysis and reactivity on reducible supports.

COMPUTATIONAL DETAILS

All calculations were performed with periodic boundary conditions using DFT methods as implemented in the CP2K package.[40,41] The exchange and correlation were accounted for by the generalized-gradient approximation with the Perdew−Burke−Ernzerhof functional.[42] Core electrons were modeled by scalar relativistic norm-conserving pseudopotentials with 4, 6, and 12 valence electrons for C, O, and Ti, respectively.[43] The valence electron wave functions were represented by a molecularly optimized double-ζ quality Gaussian basis set, and the density was expanded in terms of an auxiliary plane-wave basis with a 400 Ry energy cutoff.[44] The Brillouin zone integration was performed with a reciprocal space mesh consisting of only the Γ-point. In addition, the DFT+U method was used to describe the Ti 3d electrons on the basis of a Mulliken 3d state population analysis.[45] A U value of 13.6 eV was found to adequately reproduce the work function, W = 5.1 eV,[46] and location of defect states at 1.0 eV below the conduction band[47] (Figure S1). A more extended discussion on the choice of U parameter can be found in the Supporting Information of our recent work.[15,30] Dispersion forces, typically not well modeled by gradient-corrected functionals, are included in terms of the second generation of Grimme's[48] corrections DFT-D2, which have been shown to adequately provide a good description of potential energy surfaces for hydrocarbons on oxides[39] as well as the conformational structure and dynamics for CO_2 on TiO_2(110) and mineral surfaces.[37,49] Note that the overall description of the electronic structure obtained with the current prescription compares favorably with higher-level electronic structure methods.[50,51]

DOI: 10.1021/cs501873m
ACS Catal. 2015, 5, 1764−1771

The rutile substrate was modeled by a $TiO_2(110)$-p(2 × 6) surface slab containing 11 O−Ti−O trilayers to consider the effect of the Ti_{int} atom on the O_2 activation, as can be seen in Figure 2. These simulations were performed to assess how the addition of a high coverage of electron acceptors such as O_2 might impact the number of excess electrons available for surface redox chemistry. After accessing this issue (see Section 1) with the thicker slab, a thinner slab was used with 6 O−Ti−O trilayers to study the CO oxidation and CO_2 reduction. A 40 and 30 Å vacuum layer was added along the surface normal (z direction) of the thick and thin slabs, respectively. However, given the size of the dipole that is created during a charge transfer event, we found that even with these very large vacuum layers, the results of the simulations were severely influenced by long-range electrostatics from the periodic images. To correct for this artifact, Martyna−Tuckerman screening boundary conditions were implemented along the surface normal to screen out long-range electrostatic interactions between periodic images.[52]

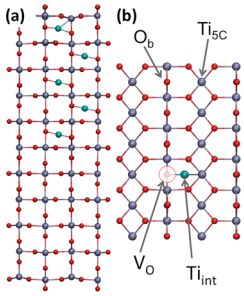

Figure 2. Illustration of TiO_2 11 trilayer slab model and demonstration of Ti interstitial (Ti_{int}), oxygen vacancy (V_O), bridge-bond oxygen (O_b) sites, and regular surface 5-coordinated Ti (Ti_{5C}) sites. (a) Side view and (b) top view; Red, blue, and dark green balls represents O, Ti, Ti_{int} atoms, respectively.

Transition states were located using the climbing image nudged elastic band method (CI-NEB) including 18 to 26 replicas.[53] Minimization of the CI-NEBs was performed by ab initio molecular dynamics, in which each replica of the NEB is given an initial temperature of 100 K and annealed to 0 K over a time scale of 1−2 ps, leading to a residual maximum component to the forces on the atoms of less than 1×10^{-3} atomic units. This approach allows us to explore the nearby configurations in phase space to obtain a path that may be substantially different (and lower in energy) than our initial conditions, but does not guarantee that we have the absolute lowest energy path connecting two intermediates. Moreover, careful inspection of the resulting reaction path indicated that in almost all cases presented here, the wave function on the two sides of the "transition state" differed by the location of a localized charge and, hence, were not adiabatically continuous. This was manifested as a cusp at the highest energy point, which was apparent only when the NEB contains a large number of replicas, as opposed to a smooth transition from reaction to products (see Figure S2 in SI). We identified this cusp as the transition point between adiabatic surfaces and performed our estimates of electron transfer kinetics relative to this configuration.

We employed Marcus theory[54,55] to consider the impact of the nonadiabatic dynamics associated with the charge transfer processes. Within this theory, the reaction rate can be obtained by the formula

$$k = \frac{2\pi}{\hbar} |V_{AB}|^2 \frac{1}{\sqrt{4\pi\lambda k_B T}} \exp\left[\frac{-(\Delta E + \lambda)^2}{4\lambda k_B T}\right] \quad (1)$$

where V_{AB} is the electronic coupling, ΔE is the energy difference between the two states, and λ is the reorganization energy shown in Scheme 1. We note that because we are considering only thermal excitations (as opposed to photo- or electrochemical), any contribution in the preexponential factor due to the population of charge carriers is not explicitly accounted for.[56]

Scheme 1. Marcus Theory Parameters for Nonadiabatic Coupling

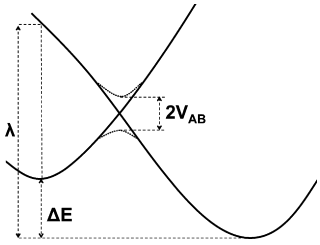

The charge-constrained DFT (cDFT) calculations were adopted to calculate the electronic coupling element (V_{AB}).[57,58] Within cDFT, two adiabatic surfaces were characterized according to the position of the electron involved in the charge transfer, defined as density-derived atomic point charge (DDAPC) and remains constrained during the wave function optimization. The reaction energy (ΔE) was then obtained as the difference between the initial state (reactant) and the final state (product) on the basis of the geometry optimization. The reorganization was described as a Condon excitation of the reactant, in which the open-shell Kohn−Sham approximation was applied to the calculation for photo-generated hole/electron excitation energies. Note that the first excitation of the highest occupied molecular orbital (HOMO) does not necessarily describe the reorganization, particularly when there are gap states occupied by excess electrons generated by intrinsic defects (excess electron from V_O). For the calculation of λ, it is important to distinguish whether an excitation occurs via an electron originating from a gap state or from the valence band, as in the case of a photogenerated electron/hole pair. An estimate of the gap state splitting can be obtained by the singlet−triplet splitting. For the calculation of $2V_{AB}$, two different charge states are assigned to the transition state configuration from a CI-NEB calculation. Defining the electronic structure of the intermediate, for example, the [$OOCO^-$] species discussed in section 2 of the Results and Discussion, is critical for both coupled electronic states treated within the cDFT method.[39] For the CO_2 reduction reaction, a simple single-triplet calculation at the transition state was sufficient to define the necessary charge state. However, for the CO oxidation reaction, a separated charge location at the C atom and at the adjacent Ti atom was found to describe the electronic transition adequately.

RESULTS AND DISCUSSION

We will first determine the number of excess electrons available for thermal surface redox reactions and how the electrostatics of

DOI: 10.1021/cs501873m
ACS Catal. 2015, 5, 1764−1771

defects like bulk Ti_{int} can impact this. Once we have quantified the available charge within the surface and charge state of the adsorbed species present at the surface, we will focus our attention on considering the role of nonadiabatic effects on the surface redox processes.

1. O_2 Adsorption and the Limit of Surface Charge. Before considering carbon oxide redox chemistry, it is necessary to consider the polaronic charge available for transfer from the surface to an adsorbate. The possible amount of surface charge available to redox processes is affected by the reduction level of the surface as determined by the nature, location, and concentration of intrinsic defects, such as oxygen vacancies (V_O) and Ti interstitial sites (Ti_{int}). It is well-known that V_O generates two excess unpaired electrons that are preferentially localized at the subsurface such that they can participate in surface reactions with ease.[14,16,18,21,59−62] On the other hand, a contribution of charge from the Ti_{int} sites is still under debate. For example, interstitial Ti defects can originate from a Ti(0) that becomes $Ti^{2+}_{(int)}$, plus two reduced lattice Ti^{3+}.[19,27,63] We recently proposed[30] that Ti_{int} thermodynamically prefers to reside in the bulk rather than near the surface in the vicinity of V_O[30] (see Figure 3). This is a result of Coulombic repulsion between the two defects that are forced to be separated from each other.[30] On the other hand, because the electrons are mobile charge carriers, the Ti_{int} will also be able to donate charge to the lattice. In this way, one might postulate that reduction of O_2 can occur even if the Ti_{int} is not present in the near vicinity, especially in the case of high coverage of strong oxidants such as O_2. Hence, it is not clear how many electrons are available at a TiO_2 surface for redox chemistry, and this aspect of the problem needs to be quantified before we can proceed to understand the charge state of the adsorbed species involved in our three-prototypical reactions.

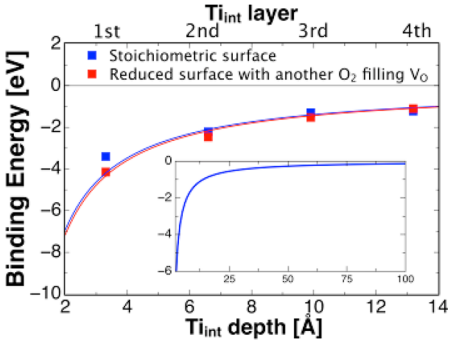

Figure 3. Adsorption energies for O_2 adsorption on the Ti_{5C} row as a function of Ti_{int} depth. A molecular adsorption is calculated on the stoichiometric surface (blue) and on the reduced surface with the V_O defect filled with another O_2 (red). Inset displays the unscreened fit for O_2 adsorption extended to a larger depth.

We follow our previous work[30] and examine the charge state of O_2 (a strong electron acceptor) upon adsorption on a vacancy-free TiO_2 surface. On a stoichiometric surface without any defects, O_2 weakly physisorbs on the surface-exposed 5-coordinated Ti (Ti_{5C}) sites. On the other hand, O_2 adsorption takes place preferentially at defect V_O sites on reduced surfaces by extracting two excess electrons, effectively becoming a strongly bound O_2^{2-}. In the presence of Ti_{int} on a surface without V_O defects, binding at the Ti_{5C} site is preferred, but the adsorption energy depends on the proximity of Ti_{int} relative to the surface (see Figure 3).[30] When it is sufficiently close to the surface (within 2 nm), charge transfer from Ti_{int} renders it an adsorbed O_2^- species.

However, the dependence of the binding energy as a function of Ti_{int} depth shows a clear Coulombic $1/r$ dependence which when extrapolated out to distances of 5−10 nm coincides with the asymptotic value of 0 eV; that is, O_2 will not bind to the surface. This implies that the favorably bound O_2^- is stabilized not by the charge transfer resulting in a stable species, but only by the electrostatic attraction of a negatively charged adsorbate and a positively charged defect. As such, we conclude that charge transfer to an adsorbed O_2 can arise from subsurface Ti_{int}, but only from those within the near vicinity (within a few nm) of the surface. Note that the current simulation does not account for the dielectric screening arising from phonon modes, ε_0, and hence, it overestimates the Coulombic stabilization.[30]

We also considered a surface with a V_O and a Ti_{int}. In addition, two O_2 were adsorbed on the surface, one O_2 at the V_O site and the other at a nearby Ti_{5C}. This setup corresponds to an O_2^{2-} bound at a V_O site, with excess electrons available only from the Ti_{int}. Note that this case corresponds to a charged state identical to that of the stoichiometric surface with a Ti_{int}, as described above but with the extra possibility that a larger concentration of O_2 may help to pull more charge out of the surface. What we find is that the adsorption energy of an O_2 at a Ti_{5C} site adjacent to an O_2^{2-} at a V_O site is essentially the same as the binding of O_2 at Ti_{5C} on a clean surface. This implies that regardless of the amount of O_2 on the surface, there is a limit of two electrons per V_O site that can become available for surface redox reactions, unless Ti_{int} or other positively charged defects are close to the surface.[14,21] However, the repulsion between V_O sites and these defects renders the probability of finding additional ones very low.[30,64,65]

Since O_2 binding on Ti_{5C} is just a weak physisorption, if another O_2 molecule occupies V_O in the absence of Ti_{int}, one can expect only a single O_2 molecule on V_O to remain above the desorption temperature of physisorbed O_2. However, the experimental observation is that up to two O_2 can be adsorbed per V_O at these temperatures.[21,26,66] One reason for this observation can be the possibility of more electrons being transferred from other intrinsic subsurface defects, that is, Ti_{int}. This assumption can be disregarded on the basis of the above analysis showing that there are only two excess electrons per V_O site available. Given a recent discussion of the possibility of an adsorbed O_4^{2-} species,[67] we also examined this scenario and found that such a species was unfavorable, decomposing to an O_2^{2-} and O_2.

Therefore, a configuration including two O_2^- (O_2^-−O_2^-) is here proposed, in agreement with Petrik and Kimmel.[66] We compare this configuration with that of an O_2^{2-} on V_O and a neutral O_2 on Ti_{5C} (O_2^{2-}−O_2^0), as shown in Figure 4a. According to the current large slab model with screening boundary condition, the O_2^-−O_2^- configuration is thermodynamically more stable than the O_2^{2-}−O_2^0 configuration by 0.32 eV. In passing, it is stressed that one obtains this configuration correctly only after scrupulously accounting for the appreciable impact of the long-range electrostatics from the periodic images (see section 2 of the Results and Discussion). Finally, it is noted that all calculations presented from this point forward in the manuscript are obtained on our thinner 6-TiO_2 trilayer slab.

The minimum energy path from the O_2^{2-}−O_2^0 to the O_2^-−O_2^- configuration, shown in Figure 4b, has only a 0.17 eV energy barrier on the basis of the CI-NEB calculation, indicating that this change should be facile, even at low

DOI: 10.1021/cs501873m
ACS Catal. 2015, 5, 1764−1771

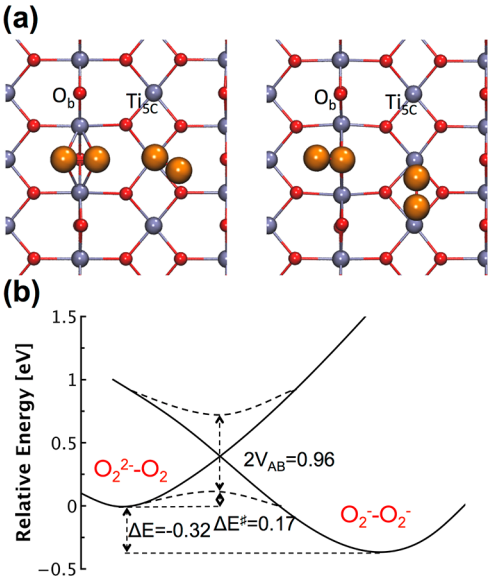

Figure 4. (a) Illustration of most stable two O_2's adsorption configuration (blue, red, and orange balls represent Ti, O from oxide, and O from adsorbed O_2 molecules, respectively; O_b and Ti_{5C} indicate bridge-bond oxygen row and 5-coordinated Ti row) and (b) adiabatic energy profile of configuration change from O_2^{2-}−O_2 to O_2^-−O_2^- configuration; ΔE, $\Delta E^{\ddagger}$, and V_{AB} represent the reaction energy, the activation energy, and the electronic coupling between two adiabatic states.

temperatures. However, we note that the configuration change involves electron transfer between two nonadiabatic, strongly coupled surfaces, which may hinder this process kinetically. Marcus theory is applied to estimate the rate of this electron transfer, taking into account the nonadiabatic coupling between the two configurations. Our estimate of the electronic coupling ($2V_{AB}$) between the adiabatic states is estimated to be 0.96 eV, which results in a relatively fast rate (∼107−1013 s^{-1}) for electron transfer in the temperature range of 100−300 K. It has been previously shown that on the rutile (110) surface,[51,54] electron transfer within the same surface layer is a fast process because of the large coupling between two adiabatic states on adjacent Ti sites. In this case, the charge transfer between the two distinguishable electronic states also occurs laterally and fast through adjacent Ti sites.

In closing this section, it is worth comparing with the case of O_2 adsorption on the anatase TiO_2 (101) surface, where the electron transfer between O_2 molecules proceeds nonadiabatically because the two analogous electronic states are poorly coupled.[22,31] On anatase TiO_2 (101), this results in adsorption of a single CO_2 molecule. Comparatively, the O_2^-−O_2^- configuration is thermodynamically the most stable configuration in the vicinity of one V_O, confirming that one V_O can stabilize up to two chemisorbed O_2's on the rutile surface, but contrary to the anatase case, this process is also kinetically feasible.

2. CO Oxidation. We now turn our attention to the CO oxidation reaction on TiO_2 surface, from coadsorbed O_2 and CO. Because of the complex dependence upon O_2 coverage[34] of the kinetics of this reaction, here we consider only the simple case in which there is a low concentration of O_2 adsorbed at a V_O site as an O_2^{2-}. For our simulation cell, this corresponds to ∼0.06 monolayer (ML) of V_O and O_2, which is comparable to that in the experiments. A CO molecule is located on Ti_{5C} site next to the adsorbed O_2, as shown in Figure 5a. In this configuration, O_2 has a peroxide-like structure (O_2^{2-}) with an O−O bond length of 1.48 Å, consistent with an O_2 molecule that has been reduced by capturing two excess electrons from V_O. CO, on the other hand, has a 1.14 Å bond length, consistent with that of a neutral CO molecule.[64]

When CO undergoes oxidation by coadsorbed O_2^{2-}, the overall reaction is completed in a two-step process. In the intermediate state, the O_2 species becomes tilted with respect to the surface normal with one O in the V_O vacancy and the other bound to the carbon of the CO at 1.48 Å (Figure 5a). The O−O bond length is 1.51 Å, consistent with an O−O single bond. The C−Ti (CO-surface) distance is now 2.25 Å, a reduction by 0.14 Å, consistent with a stronger Ti coordination bond. The other C−O bond becomes 1.2 Å, consistent with a

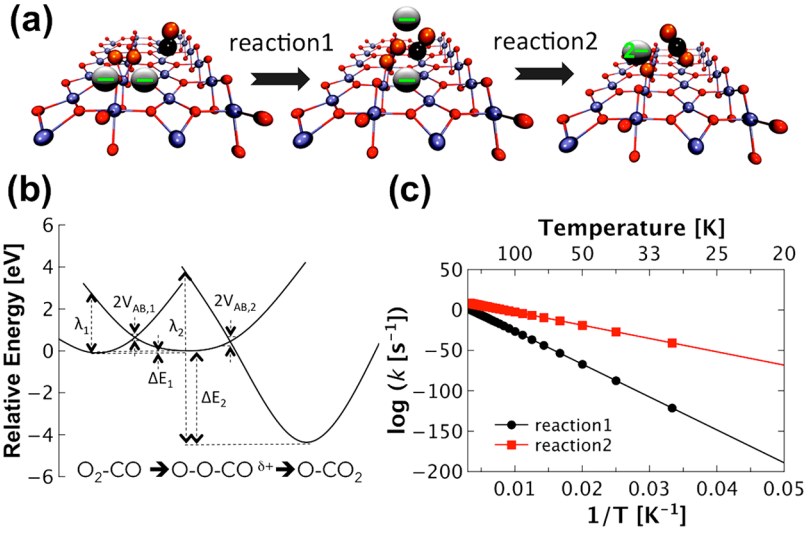

Figure 5. (a) Illustration of CO oxidation mechanism; blue, red, orange, and black balls represent Ti, O of TiO_2, O of O_2 and CO, and C atoms, respectively. The yellow "±" sign is partial charge. (b) Diabatic reaction energy profiles upon different charge states from reactant, intermediate, and product with depicted parameters used for Marcus formula (see the text). Subscript 1, 2 represent 1st and 2nd steps of overall reaction. (c) Charge transfer engaging oxidation rate in log scale.

DOI: 10.1021/cs501873m
ACS Catal. 2015, 5, 1764−1771

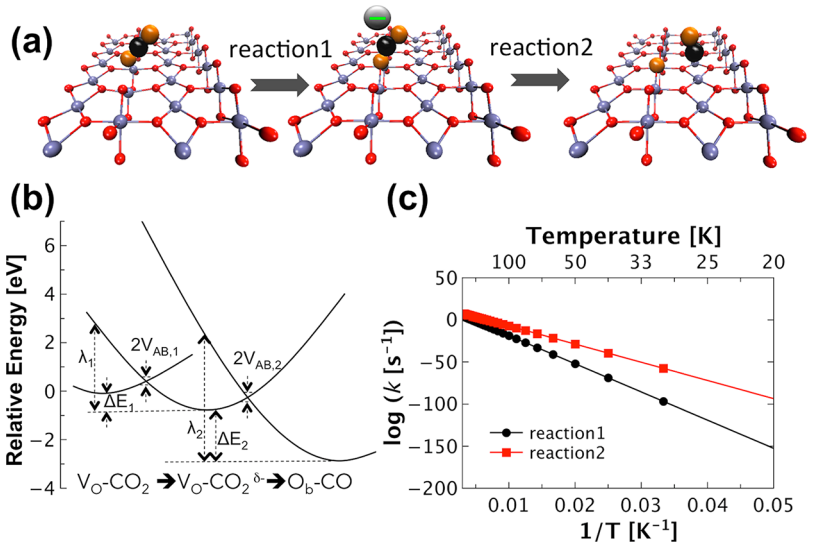

Figure 6. (a) Illustration of CO_2 reduction mechanism; blue, red, orange, and black balls represent Ti, O of TiO_2, O of CO, and C atoms, respectively. Yellow sign is negative partial charge. (b) Adiabatic reaction energy profiles upon different charge states from reactant, intermediate, and product with depicted parameters used for Marcus formula (see text). Subscripts 1, 2 represent 1st and 2nd steps of the overall reaction. (c) Charge transfer engaging reduction rate in log scale.

CO_2 moiety. Charge analysis indicates that this intermediate bears a −1 charge with the spin density delocalized over the entire $[OOCO^-]$ intermediate, a stable and almost isoenergetic species with the reactant, ΔE = 0.01 eV. At this point, the intermediate undergoes a second reaction to produce physisorbed CO_2 on a Ti_{5C} site while the remaining O^{2-} accepts an electron and heals the V_O on the surface. Note that in the first step, one electron is transferred from the O_2^{2-} adsorbate to the surface; in the second step, one electron is transferred back to create an O^{2-} species and release a neutral CO_2. To confirm this, we optimized a structure of the reactants $[O_2^{2-}:CO]$ after first removing one electron from the system. This configuration spontaneously relaxed to the corresponding $[OOCO^-]$ geometry, confirming that removal of a single charge from the surface still results in a stable intermediate.

The calculated activation energies of those two steps on the ground state surface are 0.56 and 0.34 eV for the first and second reactions, respectively. Note that the first activation energy is smaller than previous reported values[35,68] (0.83−0.87 eV), which we attribute in part to the appreciable influence of the long-range electrostatics from periodic boundary conditions. In this study, this influence was rigorously removed by screening boundary conditions. The overall barrier is smaller than the competing desorption of CO with an activation energy of 0.88 eV, which would imply this reaction could proceed thermally below the CO desorption temperature, ∼120 K; however, there is no experimental evidence of this event occurring. As discussed above, the overall reaction involves charge transfer in which two different charge states exist on the surface between the reactants and intermediate (first step) and between the intermediate and products (second step). We postulate that this may result in nonadiabatic electron transfer events that would severely hinder the rate of the CO oxidation reaction such that it will not occur below the CO desorption temperature.

Indeed, the calculated electronic coupling ($2V_{AB}$) is small enough for both reaction steps to imply a negligible influence on the nonadiabatic charge transfer process on the reaction rates. As a result, the electron transfer rate calculated from Marcus theory confirms that the reaction rates for both reactions are slow, even at high temperatures (Figure 5b,c).

The parameters required for the Marcus formula are the reaction energies (ΔE), reorganization energies (λ), and electronic coupling ($2V_{AB}$). We calculated ΔE = 0.01 and −4.36 eV, λ = 3.22 and 7.50 eV, and $2V_{AB}$ = 0.15 and 0.13 eV for the first and second reaction steps, respectively. The current CO oxidation mechanism is consistent with the observation from the photostimulated desorption experiment by Petrik and Kimmel.[34] To initiate oxidation, additional stimulation, such as photoexcitation, is required to overcome the combined relatively high thermal energy barrier and weak nonadiabatic coupling at the CO desorption temperature, ∼120 K. As a result, the photoexcited reactant $[O_2^{2-}:CO]$ can be readily converted to the intermediate $[OOCO^-]$ first, a state that is quite stable both thermodynamically and kinetically. The gradual CO_2 production observed experimentally indicates that the oxidation reaction is not a one-step reaction, and instant CO_2 production after a pause in irradiation proves the existence of an intermediate. In fact, the proposed intermediate $[OOCO^-]$ can undergo both forward and backward reactions, but both reaction rates are small enough for this state to survive for a sufficiently long time in the absence of external photostimulation. Yet, the forward reaction to produce CO_2 becomes favorable with photostimulation (see the SI and Figure S3 for more details). We should point out that this mechanism also suggests there could be a complex dependence on the wavelength of the stimulating photon. CO oxidation can proceed through a two-step mechanism involving two photoexcitations of different wavelengths or through a single step with a much higher frequency photon directly connecting the reactants to the products.

3. CO_2 Reduction. Because the role of nonadiabatic coupling is critical for CO oxidation, we examine the possibility of an analogous mechanism for thermally induced CO_2 reduction on a reduced TiO_2 surface with a V_O defect. This reaction is modeled with one CO_2 molecule adsorbed on a V_O site, as shown in Figure 6a and also proceeds in two steps. It is well-known that CO_2 binds strongly on V_O sites, tilted with

DOI: 10.1021/cs501873m
ACS Catal. 2015, 5, 1764−1771

respect to the surface normal and with a binding energy of 0.60 eV.[37,69] In this configuration, the CO_2 molecule remains effectively linear with an internal O−C−O angle of 179.8°, indicating a neutral CO_2 unaffected by the excess electrons at the V_O site. The structure of the reduction intermediate is bent with an O−C−O angle of ∼128.7°, indicating transfer of one electron from the substrate. The geometry, charge state, and spin density of this intermediate is consistent with a bound CO_2^-.[70,71] This intermediate subsequently dissociates to an O^{2-}, healing the V_O site and a CO physisorbed on a nearby Ti_{5C} site on the surface. Note that each reaction step is exothermic (see Figure 6b), and each successive configuration has an additional electron on the adsorbates.

The calculated activation energies of those two steps in thermal conditions are 0.34 and 0.33 eV, respectively. Even though a thermal reduction is expected to occur, on the basis of these activation energies at temperatures below CO_2 desorption temperature, ∼170 K,[69] CO_2 reduction to CO is not observed unless an external electrical potential is applied, such as in electron induction experiments.[36,38] This means that the rate of this reduction process is controlled by another factor, most likely by nonadiabatic coupling between two charge-transfer states. Therefore, the same approach was used for the CO oxidation process, and not surprisingly, we obtained a small electronic coupling ($2V_{AB}$) suggestive of slow electron transfer. The reaction rate and relevant model adiabatic potential energy surfaces are shown in Figure 6b,c, and the parameters used for the Marcus formula are 0.24 and 0.17 eV for electronic coupling ($2V_{AB}$), 3.94 and 6.10 eV for reorganization energies (λ), and −0.70 and −2.86 eV for the reaction energies (ΔE) for the two reaction steps. The resulting reaction rates for both steps in the series of reactions are low (see Figure 6c) such that neither event would be observed thermally below CO_2 desorption temperatures. Even in the event of an electron attachment process to generate a CO_2^- intermediate from an external source, the reverse reaction rate is also low, indicating a slow reverse reaction. This implies that the forward reaction toward CO_2 reduction is preferred (see the SI and Figure S2).

CONCLUSIONS

Studies of thermodynamically favorable reactions involving charge transfer from TiO_2 to adsorbates have been examined by means of molecular simulations and the Marcus theory of electron transfer. All processes that have been examined are thermodynamically favorable, yet not all were observed under detailed experimental scrutiny. Some reactions, such as $O_2^{2-}-O_2^0 \rightarrow O_2^- - O_2^-$, are fast and favorable as a result of strong interstate coupling. This is the result of a strong overlap between the initial and final states, which are located on the same surface layer and at proximal lattice sites. Others, such as CO oxidation and CO_2 reduction, are not fast processes because of weak coupling. Slow reactions are observed in the case of charge transfer from the bulk toward the surface. The reason for this is the poor overlap between states with very localized and well-separated charges. In such cases, the reactions can be photo- or electrochemically initiated. As a cautionary note, in these cases, indiscriminant use of CI-NEB calculations and transition state theory, as ubiquitously done in computational catalysis, to estimate rates of processes can be severely misleading. Within the CI-NEB approach, this can be rectified by the adoption of a fine granularity of the NEB grid and careful inspection of the wave function along the reaction path to identify discontinuities. In addition, inspection of the low-lying electronic states in the vicinity of the cusp will reveal the magnitude of the nonadiabatic coupling.

In the context of catalysis, this situation is unique to support materials in which charge carriers implicated in surface redox chemistry are localized. In previous studies on CO oxidation on supported metal particles such as gold,[15] or CO_2 reduction on metal surfaces such as iron,[70] charge delocalization effectively mitigates the problem. This highlights the fact that metal clusters on reducible supports can, among other things, act as a conduit for charge transfer from the support to the adsorbates, provided there is efficient coupling between the electronic states of the metal particles and the reducible oxide. This type of knowledge allows for a rational decoupling of the origin of the charge transfer in the catalytic process examining supported metal-reduced oxide systems.

ASSOCIATED CONTENT

Supporting Information

The following file is available free of charge on the ACS Publications website at DOI: 10.1021/cs501873m

(i) Test for choice of effective U parameter within DFT +U method, (ii) identification of state crossing in NEB calculations, (iii) reaction rate of backward reaction of CO oxidation and CO_2 reduction, and (iv) coordinates of the stationary points (*XYZ* format) (PDF)

AUTHOR INFORMATION

Corresponding Author

*Email: Vanda.Glezakou@pnnl.gov.

Notes

The authors declare no competing financial interest.

ACKNOWLEDGMENTS

We thank Drs. Z. Dohnalek, M. Henderson, G. Kimmel, H. Metieu, and N. Petrik for invaluable discussions. This work was supported by the U.S. Department of Energy, Office of Science and Office of Basic Energy Sciences, Division of Chemical Sciences, Geosciences & Biosciences and performed at the Pacific Northwest National Laboratory (PNNL). PNNL is a multiprogram national laboratory operated for the Department of Energy by Battelle. Computational resources were provided at EMSL, a national scientific user facility sponsored by the Department of Energy's Office of Biological and Environmental Research located at PNNL and the National Energy Research Scientific Computing Center (NERSC) at Lawrence Berkeley National Laboratory.

REFERENCES

(1) Fujishima, A.; Honda, K. *Nature* **1972**, *238* (5358), 37−38.
(2) Linsebigler, A. L.; Lu, G.; Yates, J. T. *Chem. Rev.* **1995**, *95* (3), 735−758.
(3) Ao, C. H.; Lee, S. C. *Chem. Eng. Sci.* **2005**, *60* (1), 103−109.
(4) Chen, H.; Nanayakkara, C. E.; Grassian, V. H. *Chem. Rev.* **2012**, *112* (11), 5919−5948.
(5) Adams, C.; Wang, Y.; Loftin, K.; Meyer, M. *J. Environ. Eng.* **2002**, *128* (3), 253−260.
(6) Paz, Y.; Luo, Z.; Rabenberg, L.; Heller, A. *J. Mater. Res.* **1995**, *10* (11), 2842−2848.
(7) Darouiche, R. O. *N. E. J. Med.* **2004**, *350* (14), 1422−1429.
(8) Tang, H.; Prasad, K.; Sanjinés, R.; Lévy, F. *Sens. Actuators, B* **1995**, *26* (1−3), 71−75.
(9) De Angelis, F.; Di Valentin, C.; Fantacci, S.; Vittadini, A.; Selloni, A. *Chem. Rev.* **2014**, *114* (19), 9708−9753.

DOI: 10.1021/cs501873m
ACS Catal. 2015, 5, 1764−1771

(10) Lun Pang, C.; Lindsay, R.; Thornton, G. *Chem. Soc. Rev.* **2008**, *37* (10), 2328−2353.
(11) Thomas, A. G.; Syres, K. L. *Chem. Soc. Rev.* **2012**, *41* (11), 4207−4217.
(12) Thompson, T. L.; Yates, J. T. *Chem. Rev.* **2006**, *106* (10), 4428−4453.
(13) Vittadini, A.; Casarin, M.; Selloni, A. *Theor. Chem. Acc.* **2007**, *117* (5−6), 663−671.
(14) Dohnalek, Z.; Lyubinetsky, I.; Rousseu, R. *Prog. Surf. Sci.* **2010**, *85* (5−8), 161−205.
(15) Wang, Y.-G.; Yoon, Y.; Glezakou, V.-A.; Li, J.; Rousseau, R. *J. Am. Chem. Soc.* **2013**, *135* (29), 10673−10683.
(16) Chrétien, S.; Metiu, H. *J. Phys. Chem. C* **2011**, *115* (11), 4696−4705.
(17) Deskins, N. A.; Rousseau, R.; Dupuis, M. *J. Phys. Chem. C* **2009**, *113* (33), 14583−14586.
(18) Deskins, N. A.; Rousseau, R.; Dupuis, M. *J. Phys. Chem. C* **2011**, *115* (15), 7562−7572.
(19) Deskins, N. A.; Rousseau, R.; Dupuis, M. *J. Phys. Chem. C* **2010**, *114* (13), 5891−5897.
(20) Papageorgiou, A. C.; Beglitis, N. S.; Pang, C. L.; Teobaldi, G.; Cabailh, G.; Chen, Q.; Fisher, A. J.; Hofer, W. A.; Thornton, G. *Proc. Natl. Acad. Sci.* **2010**, *107* (6), 2391−2396.
(21) Petrik, N. G.; Zhang, Z.; Du, Y.; Dohnálek, Z.; Lyubinetsky, I.; Kimmel, G. A. *J. Phys. Chem. C* **2009**, *113* (28), 12407−12411.
(22) Li, Y.-F.; Aschauer, U.; Chen, J.; Selloni, A. *Acc. Chem. Res.* **2014**, *47*, 3361−3368.
(23) Shin, S.; Metiu, H. *J. Chem. Phys.* **1995**, *102* (23), 9285−9295.
(24) Henderson, M. A.; Epling, W. S.; Peden, C. H. F.; Perkins, C. L. *J. Phys. Chem. B* **2002**, *107* (2), 534−545.
(25) Henderson, M. A.; Epling, W. S.; Perkins, C. L.; Peden, C. H. F.; Diebold, U. *J. Phys. Chem. B* **1999**, *103* (25), 5328−5337.
(26) Kimmel, G. A.; Petrik, N. G. *Phys. Rev. Lett.* **2008**, *100* (19), 196102−196106.
(27) Lira, E.; Wendt, S.; Huo, P.; Hansen, J. Ø.; Streber, R.; Porsgaard, S.; Wei, Y.; Bechstein, R.; Lægsgaard, E.; Besenbacher, F. *J. Am. Chem. Soc.* **2011**, *133* (17), 6529−6532.
(28) Pillay, D.; Hwang, G. S. *J. Chem. Phys.* **2006**, *125* (14), 144706−144706.
(29) Rasmussen, M. D.; Molina, L. M.; Hammer, B. *J. Chem. Phys.* **2004**, *120* (2), 988−997.
(30) Yoon, Y.; Du, Y.; Garcia, J. C.; Zhu, Z.; Wang, Z.-T.; Petrik, N. G.; Kimmel, G. A.; Dohnálek, Z.; Henderson, M. A.; Rousseau, R.; Deskins, N. A.; Lyubinetsky, I. *ChemPhysChem* **2014**, *16* (2), 313−321.
(31) Li, Y.-F.; Selloni, A. *J. Am. Chem. Soc.* **2013**, *135* (24), 9195−9199.
(32) Wu, X.; Selloni, A.; Nayak, S. K. *J. Chem. Phys.* **2004**, *120* (9), 4512−4516.
(33) Ji, Y.; Wang, B.; Luo, Y. *J. Phys. Chem. C* **2013**, *118* (2), 1027−1034.
(34) Petrik, N. G.; Kimmel, G. A. *J. Phys. Chem. Lett.* **2013**, *4* (3), 344−349.
(35) Kweon, K. E.; Manogaran, D.; Hwang, G. S. *ACS Catal.* **2014**, 4051−4056.
(36) Lee, J.; Sorescu, D. C.; Deng, X. *J. Am. Chem. Soc.* **2011**, *133* (26), 10066−10069.
(37) Lin, X.; Yoon, Y.; Petrik, N. G.; Li, Z.; Wang, Z.-T.; Glezakou, V.-A.; Kay, B. D.; Lyubinetsky, I.; Kimmel, G. A.; Rousseau, R.; Dohnálek, Z. *J. Phys. Chem. C* **2012**, *116* (50), 26322−26334.
(38) Tan, S.; Zhao, Y.; Zhao, J.; Wang, Z.; Ma, C.; Zhao, A.; Wang, B.; Luo, Y.; Yang, J.; Hou, J. *Phys. Rev. B* **2011**, *84* (15), 155418.
(39) Acharya, D. P.; Yoon, Y.; Li, Z.; Zhang, Z.; Lin, X.; Mu, R.; Chen, L.; Kay, B. D.; Rousseau, R.; Dohnálek, Z. *ACS Nano* **2013**, *7* (11), 10414−10423.
(40) Lippert, G.; Hutter, J.; Parrinello, M. *Mol. Phys.* **1997**, *92* (3), 477−488.
(41) VandeVondele, J.; Krack, M.; Mohamed, F.; Parrinello, M.; Chassaing, T.; Hutter, J. *Comput. Phys. Commun.* **2005**, *167* (2), 103−128.
(42) Perdew, J. P.; Burke, K.; Ernzerhof, M. *Phys. Rev. Lett.* **1996**, *77* (18), 3865−3868.
(43) Goedecker, S.; Teter, M.; Hutter, J. *Phys. Rev. B* **1996**, *54* (3), 1703.
(44) VandeVondele, J.; Hutter, J. *J. Chem. Phys.* **2007**, *127* (11), 114105.
(45) Dudarev, S.; Botton, G.; Savrasov, S.; Humphreys, C.; Sutton, A. *Phys. Rev. B* **1998**, *57* (3), 1505.
(46) Borodin, A.; Reichling, M. *Phys. Chem. Chem. Phys.* **2011**, *13* (34), 15442−15447.
(47) Yim, C.; Pang, C.; Thornton, G. *Phys. Rev. Lett.* **2010**, *104* (3), 036806.
(48) Grimme, S. *J. Comput. Chem.* **2006**, *27* (15), 1787−1799.
(49) Schaef, H. T.; Glezakou, V. A.; Owen, A. T.; Ramprasad, S.; Martin, P. F.; McGrail, B. P. *Environ. Sci. Technol. Lett.* **2013**, *1* (2), 142−145.
(50) Govind, N.; Lopata, K.; Rousseau, R.; Andersen, A.; Kowalski, K. *J. Phys. Chem. Lett.* **2011**, *2* (21), 2696−2701.
(51) Spreafico, C.; VandeVondele, J. *Phys. Chem. Chem. Phys.* **2014**, *16* (47), 26144−26152.
(52) Martyna, G. J.; Tuckerman, M. E. *J. Chem. Phys.* **1999**, *110* (6), 2810−2821.
(53) Henkelman, G.; Uberuaga, B. P.; Jónsson, H. *J. Chem. Phys.* **2000**, *113* (22), 9901−9904.
(54) Deskins, N. A.; Dupuis, M. *Phys. Rev. B* **2007**, *75* (19), 195212.
(55) Marcus, R. A.; Sutin, N. *Biochem. Biophys. Acta* **1985**, *811* (3), 265−322.
(56) Gao, Y. Q.; Georgievskii, Y.; Marcus, R. A. *J. Chem. Phys.* **2000**, *112* (7), 3358−3369.
(57) Schmidt, J.; Shenvi, N.; Tully, J. C. *J. Chem. Phys.* **2008**, *129* (11), 114110.
(58) Wu, Q.; Van Voorhis, T. *J. Chem. Phys.* **2006**, *125* (16), 164105.
(59) Kowalski, P. M.; Camellone, M. F.; Nair, N. N.; Meyer, B.; Marx, D. *Phys. Rev. Lett.* **2010**, *105* (14), 146405.
(60) Krüger, P.; Jupille, J.; Bourgeois, S.; Domenichini, B.; Verdini, A.; Floreano, L.; Morgante, A. *Phys. Rev. Lett.* **2012**, *108* (12), 126803.
(61) Pang, C. L.; Lindsay, R.; Thornton, G. *Chem. Rev.* **2013**, *113* (6), 3887−3948.
(62) Shibuya, T.; Yasuoka, K.; Mirbt, S.; Sanyal, B. *J. Phys.: Condens. Matter* **2012**, *24* (43), 435504.
(63) Wendt, S.; Sprunger, P. T.; Lira, E.; Madsen, G. K. H.; Li, Z.; Hansen, J. Ø.; Matthiesen, J.; Blekinge-Rasmussen, A.; Lægsgaard, E.; Hammer, B.; Besenbacher, F. *Science* **2008**, *320* (5884), 1755−1759.
(64) Zhao, Y.; Wang, Z.; Cui, X.; Huang, T.; Wang, B.; Luo, Y.; Yang, J.; Hou, J. *J. Am. Chem. Soc.* **2009**, *131* (23), 7958−7959.
(65) Onoda, J.; Pang, C. L.; Yurtsever, A.; Sugimoto, Y. *J. Phys. Chem. C* **2014**, *118* (25), 13674−13679.
(66) Petrik, N. G.; Kimmel, G. A. *J. Phys. Chem. C* **2010**, *115* (1), 152−164.
(67) Pillay, D.; Wang, Y.; Hwang, G. S. *J. Am. Chem. Soc.* **2006**, *128* (43), 14000−14001.
(68) Ji, Y.; Wang, B.; Luo, Y. *J. Phys. Chem. C* **2012**, *117* (2), 956−961.
(69) Acharya, D. P.; Camillone, N.; Sutter, P. *J. Phys. Chem. C* **2011**, *115* (24), 12095−12105.
(70) Glezakou, V.-A.; Dang, L. X.; McGrail, B. P. *J. Phys. Chem. C* **2009**, *113* (9), 3691−3696.
(71) Walsh, A. D. *J. Chem. Soc.* **1953**, 2260−2266.

DOI: 10.1021/cs501873m
ACS Catal. 2015, 5, 1764−1771